Journal of Membrane Science 396 (2012) 67–73

Contents lists available at SciVerse ScienceDirect

Journal of Membrane Science

journal homepage: www.elsevier.com/locate/memsci

Microfluidic NF/RO separation: Cell design, performance and application

Yair Kaufman[a,b], Roni Kasher[b], Rob G.H. Lammertink[c], Viatcheslav Freger[d,*]

[a] Albert Katz International School for Desert Studies and Unit of Environmental Engineering, Ben-Gurion University of the Negev, Sde Boqer 84990, Israel
[b] Zuckerberg Institute for Water Research, The Jacob Blaustein Institutes for Desert Research, Ben-Gurion University of the Negev, Sde Boqer 84990, Israel
[c] Soft matter, Fluidics and Interfaces, Mesa+ Institute for Nanotechnology, University of Twente, The Netherlands
[d] The Wolfson Department of Chemical Engineering, Technion – Israel Institute of Technology, Haifa, 32000, Israel

ARTICLE INFO

Article history:
Received 26 October 2011
Received in revised form
21 December 2011
Accepted 27 December 2011
Available online 12 January 2012

Keywords:
NF
RO
CFD
Microfluidic
Concentration polarization
Peptide concentration
Lévêque correlation

ABSTRACT

Microfluidics have seen a steady expansion of the operation toolbox over the last decade, which includes membrane separations as well. However, the latter are mainly limited to low-pressure operations such as dialysis, MF and UF with only very few reports focusing on high-pressure processes such as NF and RO. In this report a simple high-pressure microfluidic cell suitable for accommodating NF and RO membranes is described and critical design points are discussed. It is shown, both theoretically, using computational fluid dynamics (CFD) and Lévêque correlation, and experimentally, that a smaller height of the feed channel is beneficial for minimizing concentration polarization. Minimization of overall pressure losses, hydraulic and osmotic, indicates an optimal channel height of about 40–50 μm. The NF/RO microcell was tested as a concentrator for solution of a model peptide. The solution was successfully concentrated, however, a significant loss of peptide was observed, presumably, due to adsorption on the membrane or cell walls. This problem will need to be addressed in future studies of NF/RO microcells, however, this work demonstrates the potential and feasibility of implementing RO and NF operations in microfluidic technology.

1. Introduction

Microfluidics have recently emerged as a technology capable of handling small amounts of fluids using channels with dimensions of tens to hundreds of micrometers [1]. The small dimensions of the channel and the high surface-to-volume ratio offer advantages for applications such as chemical analysis [2,3], microreactors [4,5], biosensors [6], polymer synthesis [7], and etc. Macrofluidics have seen a steady expansion of the operation toolbox over the last decade, but many common large-scale processes are still unavailable in microfluidic format. Membrane separations and, in particular, membrane filtration, is one such field where a significant potential for novel developments and applications still exists. One advantage of the filtration processes over the other processes, such as solvent evaporation [8] or electrophoresis [9], is that they can be conveniently operate *continuously* and treat very small streams.

A large number of publications show that filtration membranes can be incorporated in microfluidic devices [10]. Many of the published studies were focused on ultrafiltration (UF) [11,12] and microfiltration (MF)[13] separations, which are driven by relatively low pressures. However, reports on incorporations in microfluidic devices of nanofiltration (NF), a process that requires high pressures (>5 bar), have been very scarce [14]. NF may retain solutes as small as 200–1000 Da favorably positioning it as an attractive separation and concentration option for important classes of biochemicals such as sugars, peptides and oligonucleotides. The latter two holds the largest promise for microfluidics, due to their high cost and small amounts used, creating a potential niche application, similar to the one filled by UF for proteins. Additionally, in analysis of environmental and pharmaceutical samples, concentration of solutions of bio-active compounds is required for proper detection [8,9]. Concentration by membranes is superior as compared to evaporation/desiccation due to mild conditions and the possibility of a continuous processing.

Implementation of NF seems to pose a few challenges. First, high pressures required for these processes are not common in microfluidics. The device then need to be very robust and tightly sealed in order to withstand the pressure and preclude leakages [10], yet preferably simple and inexpensive to manufacture. Rundel et al. have shown that pressure driven NF can be made by transmission laser welding [14]. However the membrane surface area in their module was 4 cm^2, which was fairly large, and it was not clear whether this module could be scaled down ever further. Kolfschoten et al. [15] have designed different NF microfluidic devices where the fluid runs in 500 μm wide channels and therefore the surface area of the membrane could be fairly small. Yet Kolfschoten has used *osmotic* rather than *hydraulic* pressure to drive the process therefore no conclusion can be drawn regarding the robustness and tightness of the devices.

* Corresponding author. Tel.: +972 4 8292933.
E-mail address: vfreger@tx.technion.ac.il (V. Freger).

0376-7388/$ – see front matter © 2012 Elsevier B.V. All rights reserved.
doi:10.1016/j.memsci.2011.12.052

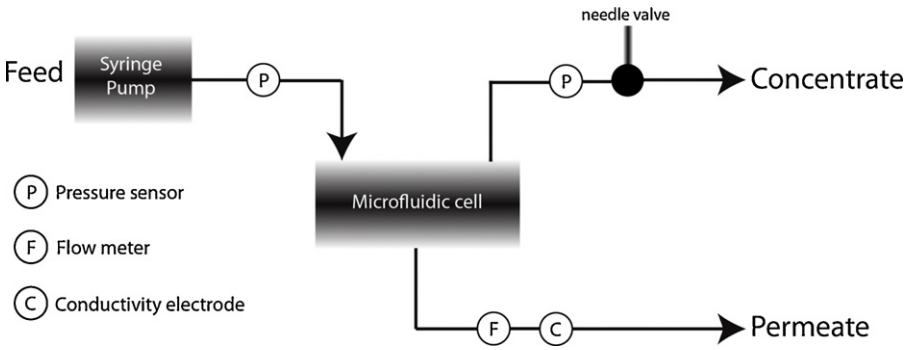

Fig. 1. Schematic presentation of the experimental setup.

Another important aspect of using NF is *concentration polarization* (CP) that can dramatically affect the solute rejection and the solvent permeation through the membrane [16]. Since the flow in microfluidics is laminar without possibility for convective mixing [10], CP may need to be carefully addressed, yet this point has not been previously examined experimentally or theoretically and remains unclear. Similarly unaddressed has been the question of optimal channel dimensions in terms of tradeoff between CP and pressure drop along the microchannel.

The present report explores the incorporation of NF in microfluidics and specifically addresses the issues of cell design, hydrodynamics and mass transfer within the cell as well as feasibility of its use for concentrating microsamples: First, a simple and robust microdevice was built that could accommodate commercial membranes and allow examining its performance. Second, transport and polarization in microfluidics are analyzed using computational fluid dynamic (CFD) results, which are compared to a simple Lévêque-type correlation. This model is subsequently used to analyze the question of optimal geometry of the microchannel and find the optimal channel height. Finally, the feasibility of using the microdevice for concentrating bio-active peptide solution is tested and associated problems, such as adsorption of peptide within the device, are discussed.

2. Materials and methods

The experimental setup is schematically depicted in Fig. 1. The feed flow was controlled by an NE-1010 syringe pump (New Era, Farmingdale, New York) with a stainless steel syringe (Hamilton, Bonaduz, Switzerland). The pressure was measured on the feed and concentrate sides using two MIDAS S05 pressure transmitters (JUMO, Canastota, New York). The permeate mass flow was measured using μ-Flow Meter (Bronkhorst, Ruurlo, Netherlands). The conductivity of the permeate was measured by a proprietary electrode cell with a cell constant 11.9 cm^{-1} and volume 5 μl. The two platinum probes were connected to PC4 potentiostat/impedance spectrometer (Gamry, Warminster, Pennsylvania) equipped with control and analysis software for physical electrochemistry and electrochemical impedance spectroscopy. The conductivity electrode was calibrated using $MgSO_4$ solutions of several known concentrations. Polyether-ether-ketone (PEEK) tubes were used (Upchurch Scientific, Oak Harbor, Washington) with the following parameters: 1/16″ outer diameter and 0.005″ inner diameter.

The microfluidic cell design is schematically shown in Fig. 2. The feed and the permeate compartments were made of two blocks poly-methyl-methacrylate (PMMA) of dimensions $2 \times 4 \times 2$ and $2 \times 4 \times 0.5$ cm^3, respectively. The channels were machined in PMMA plate using 5400 CNC mill system (Sherline, Vista, California). The feed channel was 500 μm wide and 3 cm long and two different heights, 50 and 250 μm, were used in different devices. The dimensions of the permeate channel were the same except its height was 500 μm. A PDMS spacer ~50 μm thick was spin-cast on the feed block at 2000 rpm for 1 min from poly-dimethyl-siloxane (PDMS) using a commercial RTV 615 A:B Kit (Momentive, Columbus, Ohio). The spin-cast sample was cured at 80 °C for 2 h. The whole assembly was tightened using eight 3 mm screws (not shown in Fig. 2). In order to keep the membrane supported the permeate channel was shifted laterally relative to feed channel 1 mm away from the feed channel (see cross section normal to *Z*, Fig. 2).

CFD simulations of the feed compartments were conducted using Comsol 4.0a software (COMSOL AB, Stockholm, Sweden). The

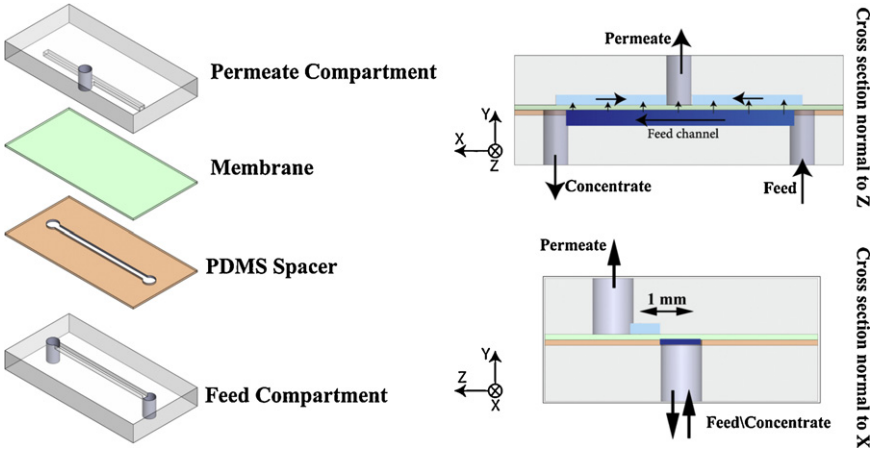

Fig. 2. Schematic illustration of the microfluidic pressure cell (not to scale).

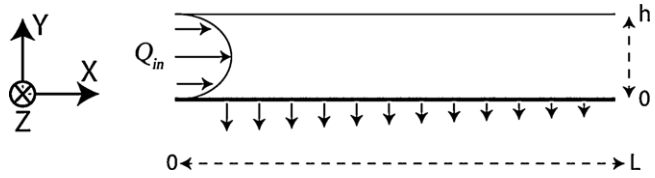

Fig. 3. Schematic drawing of the 2D geometry used to approximate the microfluidic channel. The membrane is located at $y = 0$.

following set of equations was used to describe the momentum and species balance and transport phenomena in the channel:

$$\rho(\vec{u}\cdot\nabla)\vec{u} + \nabla P - \mu\nabla^2\vec{u} = 0 \quad (1)$$

$$\nabla\cdot\vec{u} = 0 \quad (2)$$

$$D\nabla^2 C = \vec{u}\cdot\nabla C \quad (3)$$

where $\vec{u}$ is the velocity, ρ (=10^3 kg m^{-3}) is the fluid density, μ (=10^{-3} Pa s) is the dynamic viscosity, C is the solute concentration, D (=4.5×10^{-10} m^2 s^{-1}) is the effective diffusion coefficient of $MgSO_4$ [17], and P is the pressure. The pressure of the permeate was assumed to be atmospheric ($p = 0$). The boundary conditions were as follows:

$$\begin{aligned} &x = 0: \quad C_{in}, \quad P = P_{in} \\ &y = 0: \quad u_x = 0, \quad u_y = L_p(P - RTC), \quad N_0 = Cu_y(1 - R_i) \\ &y = h: \quad u_x = u_y = 0, \quad N_h = 0 \\ &x = L: \quad \frac{\partial C}{\partial X} = 0, \quad P = P_{out} \end{aligned} \quad (4)$$

where the coordinates x and y are defined in Fig. 3, L_p is the water permeability of the membrane, R is the ideal gas constant, T is the absolute temperature, $P_{in} = 4\times10^5$ Pa is the inlet pressure, P_{out} is the outlet pressure, $C_{in} = 25$ mM is the feed concentration, N_0 is the local solute flux through the membrane (i.e., at $y = 0$), u_x and u_y are the x and y components of the fluid velocity, respectively, R_i the intrinsic rejection of the membrane assumed to be constant throughout the membrane area, h and L are the height and length of the channel, respectively, and N_h is the local solute flux at $y = h$.

At $x = 0$ (inlet) the velocity profile was assumed to have the fully developed symmetric parabolic shape, i.e., the entrance effect was ignored. In addition, the edge effect associated with a finite width (z direction – 500 μm) of the channel was neglected and the problem was treated as two-dimensional, which could lead to some errors, especially, for the larger channel height yet was preferred for the sake of simplicity. Notice that the last boundary condition in Eq. (4) was reasonable since the typical Péclet number was higher than 5000. The size of the finite elements was between 2 and 30 μm.

$MgSO_4$ rejection measurements. A 25 mM aqueous solution of $MgSO_4$ (Frutarom, Haifa, Israel) in deionized water (Zalion, Petah Tickva, Israel) was pumped into the system at feed pressure 4 ± 0.1 bar. The free volume of the permeate compartment was 7.5 μl. A typical permeate flow was 0.14 μl s^{-1}, corresponding to a retention time of the permeate in the permeate compartment of about 50 s. Therefore at least 10 min were allowed after beginning of experiment before flux and rejection measurements. The observed rejection was calculated as $R_{ob} = 1 - C_p C_b^{-1}$, where C_p and C_b are the permeate and the bulk concentrations, respectively.

Peptide concentration experiments used a low-pressure reverse osmosis (LPRO) membrane ESPA 2 (Hydranautics, Vista, California) of nominal molecular weight (MW) cutoff 200 Da [18]. A peptide with the sequence IRWFFE (Peptide 55) of MW 897.05 g mol^{-1} was prepared in our laboratory by using standard solid-phase peptide synthesis methods based on the Fmoc-chemistry. Peptide 55 was purified by reverse-phase HPLC and characterized by analytical HPLC and by MALDI-TOF mass spectrometry (897.2 g mol^{-1}), as described previously [19].

Feed solution was aqueous solutions of Peptide 55 adjusted to pH 2 with 0.1 M HCl solution. The concentration of the permeate and concentrate was determined using an analytical reversed-phase HPLC chromatograph equipped with a Surveyor dual wavelength UV/Vis detector, Surveyor auto-sampler plus, Surveyor LC-pump plus (Thermo Finnigan, San-Jose, California) and a 4.6 mm × 250 mm C18 Gemini column (5 μm, 110 Å, Phenomenex, Torrance, California). HPLC analyses employed a binary gradient of 0.1% trifluoro-acetic-acid (TFA) in water (solution A) and 0.1% TFA in 75% acetonitrile in water (solution B) at a flow rate of 1.0 ml/min; HPLC solvents were obtained from J.T. Baker (Phillipsburg, New Jersey). Column effluents were monitored by UV absorbance at 220 nm.

3. Results and discussion

3.1. Microfluidic design

In choosing design and material for the NF microfluidic cells several points were considered. PMMA has been commonly used for building microfluidic devices and favorably combines the dimensional stability, good mechanical strength, low cost. Compared to other materials popular in microfluidics it is much more rigid than PDMS, yet not as fragile as glass or silicon. In addition, it is transparent and can be machined using standard manufacturing equipment. It was thus chosen based on the cost, robustness and rigidity necessary for withstanding large pressures and for ease of making and sealing the cell.

The use of commercial membranes within the cell also appears to have clear advantages. Commercial membranes have been highly optimized and are available at low cost in a variety of permeabilities and selectivities. Nevertheless, the interface between the relatively rough membrane and the rigid PMMA device does not provide efficient sealing [10]. Ikuta et al. demonstrated that micro-stereo lithography could be used to seal a UF membrane in a transparent microfluidic device [12]. However, once sealed in this way, the membrane cannot be replaced. Here it was proposed to use a PDMS layer spin-cast on top of the feed compartment, as illustrated in Fig. 2. PDMS is viscoelastic before curing therefore it effectively fills the microscopic gaps between PMMA surface and NF/RO membrane. A thickness of PDMS layer of ~50 μm was found to be optimal to prevent leakage on one hand and avoid blocking the channel by PDMS on the other hand. This kind of sealing allows an easy membrane replacement without the need to discard the whole cell.

Supporting the membrane properly is another crucial aspect. Standard solutions such as the use of a supporting mesh or microporous media are unsuitable or unfavorably complicate making of microchannels. On the other hand, applying a high pressure directly to an unsupported membrane placed over an open permeate channel holds the high risk of damaging the membranes, especially, at the sharp channel edges. A simple solution employed here was to displace the permeate channel laterally by 1 mm relative to the feed channel (see Fig. 2). The membrane is then robustly supported by the solid PMMA surface, forcing the permeate to flow about 1 mm laterally rather than across the supporting porous layer of the membrane. This distance is 5–10 times larger than the support thickness and increases the support resistance. Yet, given the fact that the support resistance is 2–3 orders of magnitude lower than that of the toplayer and lateral permeate flow should mostly occur within the thick and highly permeable bottom part of the support, the expected increase in the hydraulic resistance was negligible. Indeed, no significant change was found in the water permeability, as compared to the regular lab-scale setup (see next).

The proposed NF microcell design is simple and requires only most basic fabrication facilities and inexpensive materials. The tests

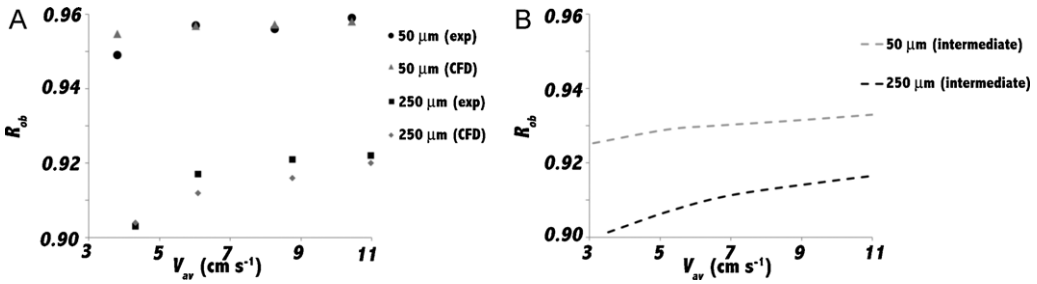

Fig. 4. Observed rejection of $MgSO_4$ vs. average feed velocity in the channel. (A) Shows the measured and the calculated (CFD) rejection of NF-270 in two different channels. The CFD simulations used experimentally determined input parameters $R_i = 0.955$ and $L_p = 11.5\,l\,m^{-2}\,h^{-1}\,bar^{-1}$ for 50 μm channel and $R_i = 0.970$ and $L_p = 14.7\,l\,m^{-2}\,h^{-1}\,bar^{-1}$ for 250 μm channel. (B) Shows the calculated (CFD) R_{ob} in two different channels (50 and 250 μm) (see Section 3.2) using *the same* intermediate values $R_i = 0.964$ and $L_p = 13.1\,l\,m^{-2}\,h^{-1}\,bar^{-1}$.

showed that it withstands pressures up to at least 16 bar (the upper limit of pressure sensors used) and allows easy incorporation of any flat-sheet membrane, as well as membrane replacement. To verify that the membrane performs in the microdevice similar to regular laboratory cell, a commercial NF membrane (NF-270) was examined in two different microfluidic NF cells, differing by their heights (50 and 250 μm). The rejection of $MgSO_4$ was measured for different feed velocities. Fig. 4A shows that the maximum observed rejection, R_{ob}, in 250 μm channel was about 0.92 whereas in the 50 μm channel it was about 0.96. The water permeability was 11.7 and $14.5\,l\,m^{-2}\,h^{-1}\,bar^{-1}$, respectively. These results, somewhat different for two cells, as common for small membrane samples, compare well with the typical performance measured in laboratory cells [20,21], which suggests that the membrane maintained integrity within the microcell.

3.2. Mass transfer and concentration polarization in the micro-channel

A simple model of mass transfer in a membrane (micro) channel is the classic Lévêque correlation that yields the average mass transfer coefficient in the channel, k, as a function of channel dimensions and average velocity as follows:

$$k = \frac{D}{\delta} = a\left[\frac{D^2}{L}\right]^{0.33}\left[\frac{V_{av}}{d_h}\right]^{0.33} \tag{5}$$

$$d_h = \frac{4wh}{2(w+h)} \tag{6}$$

where $a = 1.85$, d_h is the hydraulic diameter of the channel, w is the channel width, and V_{av} is the average velocity of the solvent in the channel (averaged along x). The correlation holds for a laminar flow in a rectangular channel, which was the case here (*Re* was of the order of 10 in all experiments).

It is easily seen that the Lévêque correlation predicts that for a given length a narrower channel would lead to a higher k hence smaller concentration polarization. Regardless of whether channels are compared for the same velocity or feed flow rate, k would increase when the channel gets narrower, since d_h decreases and V_{av} either stays constant or increases. Indeed, a higher rejection in the smaller channel is clearly seen in experimental results presented in Fig. 4A.

To see it more explicitly and also validate the Lévêque correlation in microchannels in presence of a trans-membranes flow, CFD calculations were carried out. The intrinsic rejection R_i, an input parameter required for CFD simulations, was calculated using following linearized equation:

$$\ln\left(\frac{R_{ob}}{1-R_{ob}}\right) = \ln\left(\frac{R_i}{1-R_i}\right) - \frac{j_v}{k} \tag{7}$$

Using several experimental values of R_{ob} and j_v measured for the same cell and membrane and Eq. (5) for k, the value of R_i was calculated from the intercept of the linear plot of $\ln(R_{ob}/(1-R_{ob}))$ vs. j_v/k. The input parameters for CFD were then the intrinsic rejection R_i, inlet and outlet pressures P_{in} and P_{out}, and inlet concentration C_{in}. For the sake of simplicity R_i was assumed to be constant throughout the membrane surface though it is in general concentration- and flux-dependent [22]. This assumption was reasonable, given the purpose of this study and fairly moderate variations of concentration and flux along the channel in the present experiments. The output was the permeate flux rate j_v, permeate concentration C_p, overall rejection $R_{ob} = 1 - C_p C_b^{-1}$, average concentration on the membrane surface $\bar{C}_m$, and the average mass transfer coefficient k calculated as follows:

$$j_v = \frac{w}{A}\int_0^L v_y\,dL \tag{8}$$

$$C_p = \frac{w}{J_v A}\int_0^L v_y C_m(1-R_i)\,dL \tag{9}$$

$$\bar{C}_m = \frac{C_p}{1-R_i} \tag{10}$$

$$k = \frac{J_v}{\ln(\bar{C}_m/\bar{C}_b)} \tag{11}$$

where A is the membrane surface area ($1.5\times10^{-5}\,m^2$) and v_y and C_m are, respectively, normal component of the fluid velocity (local volume flux) and local concentration at the membrane surface obtained in CFD simulations.

The results displayed in Fig. 4A show a good correlation between CFD predictions and experiment. The maximum deviation between the simulations and measurements was under 10% and apparently the simplified 2D geometry assumed in simulations did not result in a significant error. Fig. 5 explicitly compares the values of k based on CFD and Eq. (5). It is seen that the Lévêque correlation adequately agrees with CFD results, which justifies the use of the former for estimating R_i and for optimization of channel size in the next section.

Note that the values of R_i and L_p deduced from experiment were slightly different for the membranes used in cells with channel height 250 and 50 μm (see Fig. 4). Such variations are common for small membrane samples, however, they superimpose on differences resulting from different channel height and concentration polarization. To explicitly see the differences due to channel height only the simulations were repeated for the two channels using identical values $L_p = 13.1\,l\,m^{-2}\,h^{-1}\,bar^{-1}$ and $R_i = 0.964$ for both channels (50 and 250 μm), intermediate to L_p and R_i actually measured for the two channels. The results are displayed in Fig. 4B (dash lines). Expectedly, a smaller yet significant difference in R_{ob} was still obtained, now due only to the better performance of the smaller

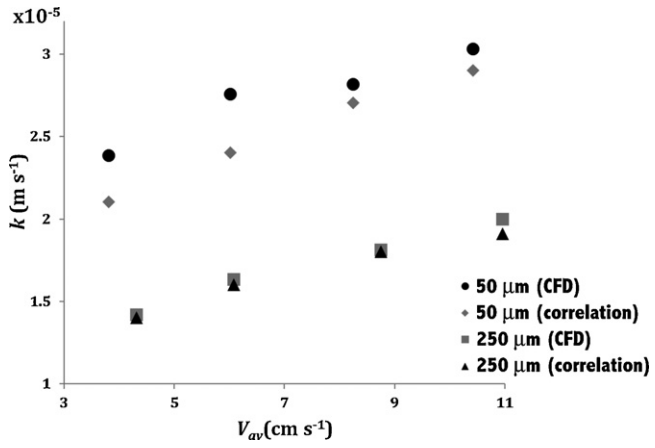

Fig. 5. Mass transport coefficient estimated using CFD and Lévêque correlation.

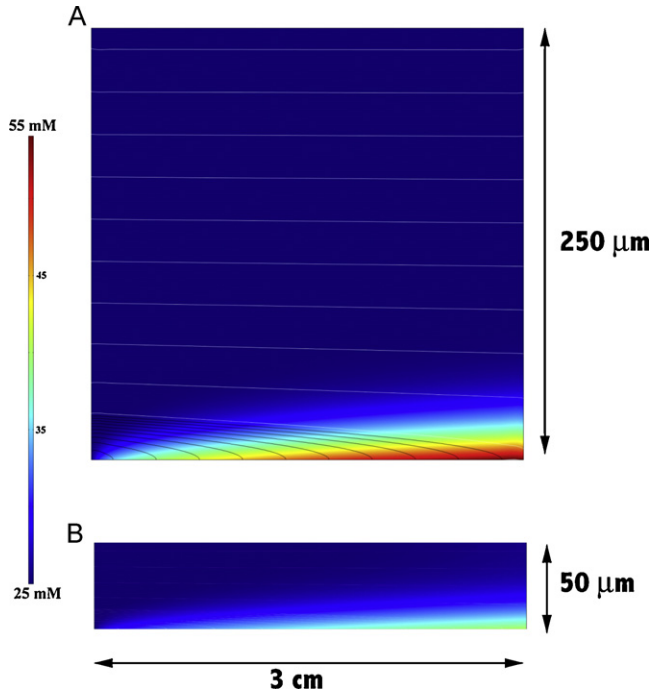

Fig. 6. Concentration field of $MgSO_4$ in 250 μm channel height (A) and in 50 μm channel height (B). The curved lines in (A) are stream lines of the solvent. V_{in} = 0.045 m s^{-1}, R_i = 0.964, and L_p = 13.1 l m^{-2} h^{-1} bar^{-1}.

channel. This difference is most explicitly seen in Fig. 6 that displays the computed concentration profiles within the cell for two channel heights and the same average R_i and L_p and the inlet velocity V_{in} = 0.045 m s^{-1}. A significantly thinner diffusion boundary later for the smaller channel height is clearly visible and once again confirms that mass transport is enhanced and polarization reduced in a shallower channel.

3.3. Optimization of channel height

An interesting question, complementary to the analysis of mass transport and relevant to design of microfluidic NF and RO cells, is the optimal channel height. When the feed microchannel is milled, as in this study, its height is far easier to vary than, e.g., width that is determined by the mill diameter. When a certain volume of solution is to be treated, reduction of the channel height will help reduce concentration polarization (see above). However it will also lead to a larger loss of pressure along the channel and reduce the average trans-membrane pressure and rejection. In a simple example of an ideally rejecting membrane and concentrated salt solution, the main result of CP may be viewed as a loss of the driving force due to increased osmotic pressure at the upstream membrane surface. In actual microfluidic operations the reduced driving force and rejection might be partly compensated with a higher inlet pressure and a higher flow rate. However, the different parameters are not independent and a higher flow rate will be at the cost of a lower concentration factor and a higher pressure will increase the energy consumption (important for, e.g., battery-powered systems) and require a more demanding design. Therefore, as a simple example, a problem may be considered of minimizing the *total lost trans-membrane pressure* P_L defined as follows:

$$P_L(h) = \Delta P_f + \Delta\pi \tag{12}$$

Here the first term is the pressure drop along the channel and the second is the osmotic pressure increase due to CP. The first term may be estimated using the Hagen–Poiseuille equation for a rectangular channel and the second one using the van't Hoff equation, in which the concentration on the membrane surface C_m is corrected for CP, i.e., [16,23].

$$\Delta P_f = 32\mu L \frac{V_{av}}{{d_h}^2} \tag{13}$$

$$\Delta\pi = RT(C_m - C_p) \tag{14}$$

where

$$C_m = C_b \exp\left[\frac{J_v}{k}\right] \tag{15}$$

$$j_v = L_p(\Delta P - \Delta\pi) \tag{16}$$

Both $\Delta\pi$ and P_L in Eq. (12) are affected by the average velocity and channel height in opposite manner. This trade-off calls for geometry optimization. Fig. 7A plots P_L (h) for representative conditions yielding a minimum at about h = 40 μm. Fig. 7B shows that the C_m and the thickness of diffusion boundary layer, δ, decrease monotonically as the channel height decreases. Obviously, the location of the minimum in Fig. 7A will vary with the volume rate and feed concentration, i.e., the osmotic pressure of the feed. Nevertheless, the very sharp dependence of the pressure drop on channel height, as opposite to moderate variation of boundary layer thickness ad CP (Fig. 7B), suggests that the optimal height could be not far from 50 μm, the smaller height used in this study. Given the sharp dependence of $\Delta\pi$, the optimal height might change, but probably not much, if the optimization criterion needs to consider the loss of rejection due to CP in addition to loss of flux.

3.4. Concentration of peptide solutions: demonstration and performance evaluation

As stated in Section 1, concentration and separation of minute amounts of peptides in small samples is one promising application for the microfluidic version of NF/RO. To examine the feasibility of this application the NF cell was used to concentrate a solution of Peptide 55, a synthetic bio-active peptide that belongs to the family of peptides with estrogen-like activity [19]. A peptide solution of 0.06 mg ml^{-1} was used, and in each experiment the solution was concentrated to a different degree by varying the feed rate relative to the permeate rate. The former was varied through the settings of the feed pump, while the latter mainly depended on the feed pressure controlled by the needle valve.

The degree of concentration could be measured in two ways: (1) as the ratio of the measured peptide concentrations in the concentrate and feed (concentration factor), and (2) the ratio between the concentrate and feed weights (weight factor). Fig. 8 compares between concentration factor and the weight factor. The figure

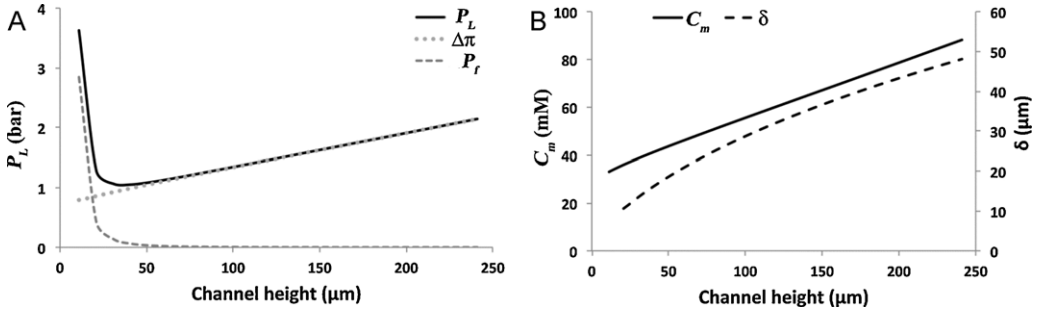

Fig. 7. Total pressure loss (P_L) vs. channel height in (A). CP and δ vs. channel height in (B). The volumetric feed was 3 ml h^{-1}, L and channel width (w) were 0.03 m and 500 μm, respectively, L_p = 11 l m^{-2} h^{-1} bar^{-1}, $D = 4.5 \times 10^{-10}$ m^2 s^{-1} (diffusion coefficient of $MgSO_4$) [17], J_v = 38.7 l m^{-2} h^{-1}, ΔP = 4 bar, and R_i = 0.97.

shows that in all experiments the concentration factor was smaller than the weight factor, the discrepancy increasing with degree of concentration.

The observed discrepancy between weight factor and HPLC-measured concentration factor could be due to permeation, adsorption, or degradation of the peptide. The possibility of permeation could apparently be ruled out, since no peptide could be detected in the permeate for all feed concentrations used (0.06–1.8 mg ml^{-1}). It was confirmed that the detection limit of HPLC did not exceed 0.018 mg ml^{-1} therefore the rejection in all cases was larger than 70% and apparently very close to 100%. Even assuming that permeate concentration was just below the detection limit, the peptide loss to permeate would only be a small fraction (<15%) of the missing peptide. The high peptide rejection was consistent with the molecular weight of the peptide that was much larger than the cutoff of the membrane used (a low-pressure RO membrane ESPA2). Degradation of the peptide during the experiment was also ruled out by testing Peptide 55 stability in pH 2 by injecting peptide samples to analytical HPLC in specific time intervals; no significant change in peptide concentration was observed over 6 h, the time of the longest filtration experiment.

On the other hand, adsorption of the peptide on the membrane or on other system parts was likely, since many organic compounds tend to adsorb onto the crosslinked aromatic polyamide layer of NF and RO membranes [24]. The adsorption mechanism is supported by Fig. 9 that shows the amount of missing peptide (the amount in the feed minus that in permeate) vs. the logarithmic average of the bulk concentration C_{av}, i.e.:

$$C_{av} = \frac{C_{in} - C_c}{\ln(C_{in}/C_c)} \tag{17}$$

where C_c is the concentrate concentration.

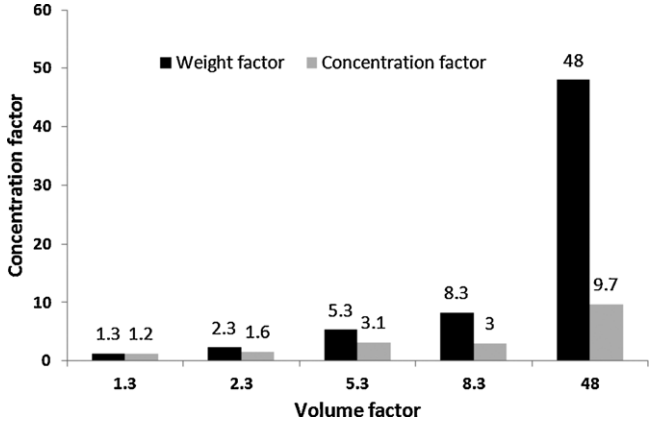

Fig. 8. Peptide concentration factor vs. solvent weight factor.

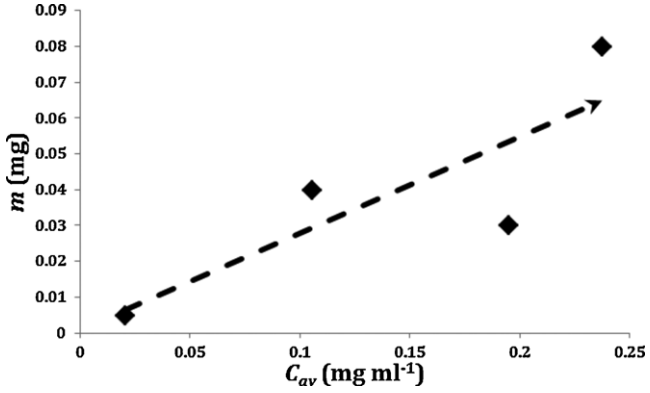

Fig. 9. The peptide loss in each experiment vs. the average concentration in the channel.

The logarithmic average is the appropriate average in cases when concentration varies along the channel and adsorption obeys a linear isotherm and linear kinetics [25]. Indeed Fig. 9 shows that the amount of missing (adsorbed) peptide and solution concentration correlate approximately linearly. It is important to note that the adsorption could take place both on the membrane and the channel walls, since several publications have shown that PMMA [26] and PDMS [27] may adsorb peptides and proteins.

These results indicate that adsorption of solutes on the membrane, channel walls, and other parts of the system (tubing, pump etc.) could be a major challenge in using NF/RO microfluidics for concentration and separation of dilute peptide solutions. One possible way to cope with this problem could be to use more inert materials for parts that have a contact with the solution. Another option could be to modify the inner surfaces and membrane, since it was shown that by modifying surfaces, e.g., via PEG grafting [26], protein and peptides adsorption can be dramatically reduced.

4. Conclusions

NF and RO membranes were successfully introduced in microfluidic device using relatively simple techniques and inexpensive materials and important design points were discussed. The preparation of a robust tightly sealed device was successful using rigid materials such as PMMA and PDMS as a sealant.

It was shown that Lévêque correlation predicts fairly adequately the mass transport coefficient in microfluidic channel. In particular, the correlation as well as CFD simulations show that CP is depressed as the hydraulic diameter decreases. This trend was also confirmed by experiments with $MgSO_4$. Minimization of overall pressure losses, hydraulic and osmotic due to CP, indicates an optimal channel height of about 40–50 μm.

The performance of the microfluidic device was also experimentally evaluated for concentrating dilute peptide solutions. The peptide solution was successfully concentrated, which demonstrates that a microfluidic operation of NF or RO is a promising and feasible option for this and similar applications. However, observed loss of peptide apparently indicates that it was adsorbed on the inner surface of the cell (NF membrane, PMMA and/or PDMS). This seems to be a major challenge that may have to be addressed in the future, e.g., via appropriate selection of materials or surface modification.

Acknowledgments

Y. K. thanks the membrane technology group at the University of Twente for kindly hosting him and generously sharing the knowledge and expertise in microfluidics. Marina Yamit-Lutskiy is acknowledged for the help with HPLC analysis of the peptide.

References

[1] G.M. Whitesides, The origins and the future of microfluidics, Nature (London) 442 (2006) 368.
[2] A.J. Demello, Control and detection of chemical reactions in microfluidic systems, Nature 442 (2006) 394.
[3] Y. Xiang, Y. Lu, Using personal glucose meters and functional DNA sensors to quantify a variety of analytical targets, Nat. Chem. 3 (2011) 697.
[4] O. Wörz, K. Jäckel, T. Richter, A. Wolf, Microreactors, a new efficient tool for optimum reactor design, Chem. Eng. Sci. 56 (2001) 1029.
[5] G.N. Doku, W. Verboom, D.N. Reinhoudt, A. van den Berg, On-microchip multiphase chemistry – a review of microreactor design principles and reagent contacting modes, Tetrahedron 61 (2005) 2733.
[6] D.A. Boehm, P.A. Gottlieb, S.Z. Hua, On-chip microfluidic biosensor for bacterial detection and identification, Sens. Actuators B: Chem. 126 (2007) 508.
[7] D. Dendukuri, K. Tsoi, T.A. Hatton, P.S. Doyle, Controlled synthesis of nonspherical microparticles using microfluidics, Langmuir 21 (2005) 2113.
[8] O. Vorm, P. Roepstorff, M. Mann, Improved resolution and very high sensitivity in MALDI TOF of matrix surfaces made by fast evaporation, Anal. Chem. 66 (1994) 3281.
[9] A. Wainright, S.J. Williams, G. Ciambrone, Q. Xue, J. Wei, D. Harris, Sample preconcentration by isotachophoresis in microfluidic devices, J. Chromatogr. A 979 (2002) 69.
[10] J. de Jong, R. Lammertink, M. Wessling, Membranes and microfluidics: a review, Lab Chip 6 (2006) 1125.
[11] Y. Jiang, P.C. Wang, L.E. Locascio, C.S. Lee, Integrated plastic microfluidic devices with ESI-MS for drug screening and residue analysis, Anal. Chem. 73 (2001) 2048.
[12] K. Ikuta, S. Maruo, T. Fujisawa, A. Yamada, Micro Concentrator with Opto-Sense Micro Reactor for Biochemical IC Chip Family. 3D Composite Structure and Experimental Verification, 1999, p. 376.
[13] I.S. Ngene, R.G.H. Lammertink, M. Wessling, W. van der Meer, A microfluidic membrane chip for in situ fouling characterization, J. Membr. Sci. 346 (2010) 202.
[14] J.T. Rundel, B.K. Paul, V.T. Remcho, Organic solvent nanofiltration for microfluidic purification of poly (amidoamine) dendrimers, J. Chromatogr. A 1162 (2007) 167.
[15] R.C. Kolfschoten, A.E.M. Janssen, R.M. Boom, Mass diffusion-based separation of sugars in a microfluidic contactor with nanofiltration membranes, J. Sep. Sci. 34 (2011) 1338.
[16] M. Mulder, Basic Principles of Membrane Technology, Springer, 1996.
[17] D. Lide, CRC Handbook of Chemistry and Physics, 2009 (Internet Version).
[18] C. Bellona, J.E. Drewes, G. Oilker, J. Luna, G. Filteau, G. Amy, Comparing nanofiltration and reverse osmosis for drinking water augmentation, J. Am. Water Work. Assoc. 100 (2008) 102.
[19] R. Kasher, B. Gayer, T. Kulik, D. Somjen, N. Venkatesh, M. Fridkin, et al., Design, synthesis, and evaluation of peptides with estrogen-like activity, Biopolym. Pept. Sci. 76 (2004) 404.
[20] S. Belfer, J. Gilron, N. Daltrophe, Y. Oren, Comparative study of biofouling of NF modified membrane at SHAFDAN, Desalination 184 (2005) 13.
[21] M. Manttari, A. Pihlajamaki, M. Nystrom, Effect of pH on hydrophilicity and charge and their effect on the filtration efficiency of NF membranes at different pH, J. Membr. Sci. 280 (2006) 311.
[22] S. Bason, Y. Kaufman, V. Freger, Analysis of ion transport in nanofiltration using phenomenological coefficients and structural characteristics, J. Phys. Chem. B 114 (2010) 3510.
[23] O. Kedem, A. Katchalsky, A physical interpretation of the phenomenological coefficients of membrane permeability, J. Gen. Physiol. 45 (1961) 143.
[24] M. Williams, J. Hestekin, C. Smothers, D. Bhattacharyya, Separation of organic pollutants by reverse osmosis and nanofiltration membranes: mathematical models and experimental verification, Ind. Eng. Chem. Res. 38 (1999) 3683.
[25] S. McCabe, J. Smith, Harriott, Unit Operations of Chemical Engineering, McGrawhill International Editions, 1993.
[26] J. Liu, T. Pan, A.T. Woolley, M.L. Lee, Surface-modified poly (methyl methacrylate) capillary electrophoresis microchips for protein and peptide analysis, Anal. Chem. 76 (2004) 6948.
[27] S. Hu, X. Ren, M. Bachman, C.E. Sims, G. Li, N. Allbritton, Cross-linked coatings for electrophoretic separations in poly (dimethylsiloxane) microchannels, Electrophoresis 24 (2003) 3679.